analytical chemistry

pubs.acs.org/ac Article

Centrifugal Microfluidic Method for Enrichment and Enzymatic Extraction of Severe Acute Respiratory Syndrome Coronavirus 2 RNA

Rachelle Turiello,* Leah M. Dignan, Brayton Thompson, Melinda Poulter, Jeff Hickey, Jeff Chapman, and James P. Landers

Cite This: *Anal. Chem.* 2022, 94, 3287−3295 Read Online

ACCESS | Metrics & More | Article Recommendations | Supporting Information

ABSTRACT: The diversification of analytical tools for diagnosis of severe acute respiratory syndrome coronavirus 2 (SARS-CoV-2) is imperative for effective virus surveillance and transmission control worldwide. Development of robust methods for rapid, simple isolation of viral RNA permits more expedient pathogen detection by downstream real-time reverse transcriptase polymerase chain reaction (real-time RT-PCR) to minimize stalled containment and enhance treatment efforts. Here, we describe an automatable rotationally driven microfluidic platform for enrichment and enzymatic extraction of SARS-CoV-2 RNA from multiple sample types. The multiplexed, enclosed microfluidic centrifugal device (μCD) is capable of preparing amplification-ready RNA from up to six samples in under 15 min, minimizing user intervention and limiting analyst exposure to pathogens. Sample enrichment leverages Nanotrap Magnetic Virus Particles to isolate intact SARS-CoV-2 virions from nasopharyngeal and/or saliva samples, enabling the removal of complex matrices that inhibit downstream RNA amplification and detection. Subsequently, viral capsids are lysed using an enzymatic lysis cocktail for release of pathogenic nucleic acids into a PCR-compatible buffer, obviating the need for downstream purification. Early in-tube assay characterization demonstrated comparable performance between our technique and a "gold-standard" commercial RNA extraction and purification kit. RNA obtained using the fully integrated μCDs permitted reliable SARS-CoV-2 detection by real-time RT-PCR. Notably, we successfully analyzed full-process controls, positive clinical nasopharyngeal swabs suspended in viral transport media, and spiked saliva samples, showcasing the method's broad applicability with multiple sample matrices commonly encountered in clinical diagnostics.

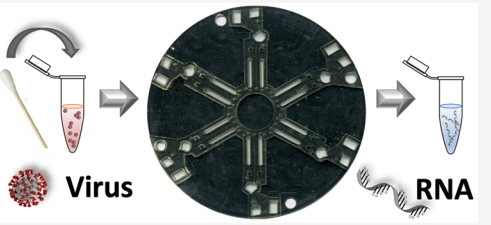

Severe acute respiratory syndrome coronavirus 2 (SARS-CoV-2) was determined to be the causative agent of the COVID-19 pandemic in December of 2019.[1] Since then, the most ubiquitous laboratory method for diagnostic testing and surveillance monitoring has been real-time reverse transcriptase polymerase chain reaction (real-time RT-PCR) amplification of viral RNA.[2] RT-PCR is recognized as a robust technique with high analytical sensitivity and target specificity; however, detection depends directly on successful upstream RNA isolation from crude samples. In the case of viral pathogens, this involves lysis of virion envelopes followed by purification of the liberated RNA. "Gold-standard" RNA isolation methods require sample incubation with lytic enzymes, followed by RNA purification via flow through a packed column or silica beads suspended in the lysate.[3] While these methods are ostensibly successful, practical challenges remain, including high cost and supply chain limits. Specifically, reliance on a narrow panel of viral NA preparation techniques during an epidemiological outbreak is problematic, as the availability of conventional kits may become limited.[4] Furthermore, their time-consuming, labor-intensive workflows require multiple open-tube washing and transfer steps, making many kits susceptible to sample contamination, analyst exposure, and nucleic acid (NA) loss.[5] Thus, complete reliance on gold standard RNA extraction methods may ultimately be detrimental to the effectiveness of surveillance and transmission control due to stalled containment and/or treatment efforts.[6]

Beyond the aforementioned limitations, conventional methods for RNA isolation do not involve a mechanism for upstream virion enrichment, leveraging either centrifugation, nuclease treatment, or affinity capture particles to improve detection sensitivity.[7,8] Enrichment is particularly advantageous for low titer samples in which preconcentration of the target analyte could mean the difference between detection and a negative result.[9] Furthermore, many enrichment methods facilitate the removal of sample matrices, often containing products that may influence sample extraction and

Received: December 1, 2021
Accepted: January 31, 2022
Published: February 9, 2022

https://doi.org/10.1021/acs.analchem.1c05215
Anal. Chem. 2022, 94, 3287−3295

hinder detection.[10,11] In essence, inclusion of a method for virion enrichment and matrix removal may increase the effectiveness of RNA extraction and improve the assay sensitivity. Recently, successful virion enrichment from multiple matrices has been demonstrated using affinity-capture hydrogel Nanotrap particles.[9] Composed of cross-linked polymer networks, these nanoparticles (NPs) are decorated with chemical affinity baits that promote virion capture via interactions with viral surface spike proteins.[12] Nanotrap enrichment, in conjunction with one-step enzymatic extraction, has proved successful in detecting SARS-CoV-2 from clinical nasopharyngeal swabs, surveillance sample mimics, and contrived saliva samples.[13]

To address the shortcomings of conventional RNA isolation, we propose a multiplexed microfluidic centrifugal device (μCD) for expedited, automated virion enrichment and enzymatic extraction of SARS-CoV-2 RNA from clinical samples. Specifically, NP-based enrichment is coupled with a rapid, single-step method for virion lysis of PCR-ready RNA.[14,15] Each μCD contains six domains for parallel processing in an enclosed format that mitigates the risk of contamination and analyst exposure to SARS-CoV-2. Reliance on rotationally driven flow eliminates the need for bulky external hardware (e.g., syringe pumps), enabling the creation of smaller, field-forward instrumentation.[16,17] Notably, the NPs are functionalized with iron oxide, allowing for efficient mixing in the system via application of an external, bidirectional rotating magnetic field (bRMF) that facilitates NP "sweeping".[18] Furthermore, active, laser-actuated valving permits both valve opening and channel closures to enable reliable implementation of numerous sequential unit operations.[19] Here, we demonstrate the compatibility of our optimized method for rapid SARS-CoV-2 sample preparation with full-process controls and clinical samples in multiple, clinically relevant matrices.

MATERIALS AND METHODS

Clinical Sample Preparation and Analysis. Nasopharyngeal clinical specimens were collected, prepared, and tested by real-time RT-PCR at the University of Virginia Health System for subject diagnosis and stored at −20 °C in a viral transport medium (VTM). Prior to receipt, samples were deidentified according to the IRB-approved protocol. Standard of care testing was performed with methods granted emergency use authorization (EUA) from the FDA according to manufacturer's instructions, these included the Abbott-Alinity-m SARS-CoV-2 assay, the Abbott M2000 Real-Time SARS-CoV-2 assay, and the Xpert Xpress SARS-CoV-2 assay. For analysis, each sample was vortexed for 10 s, and 600 μL of liquid was transferred to a 2 mL screw-cap microcentrifuge tube. VTM samples were inactivated by heating for 30 min at 65 °C, transferred to a sealed bag, and stored at −80 °C until further analysis.

Sample Materials. Any sample assigned a cycle threshold (C_t) value by the clinical laboratory was considered positive for SARS-CoV-2; C_t values were used to determine relative viral titers. A SARS-CoV-2 reference material (100 000 copies/mL, AccuPlex SARS-CoV-2 Reference Material, SeraCare, Milford, MA) was diluted from 100 copies/μL to 50 and 25 copies/μL in either PCR-grade water (Molecular Biologicals International, Inc.), clinically negative SARS-CoV-2 samples in VTM, or human saliva to serve as on-disc full-process analytical controls.

In-Tube Nanotrap Enrichment and RNA Extraction. In-tube studies were completed with 100 μL of inactivated clinical samples at high, moderate, and low viral titers. Nanotrap Magnetic Virus Particles (CERES Nanosciences, Inc., Manassas, VA) were spiked into SARS-CoV-2 clinical samples and full-process controls at 5, 10, 20, 30, or 50% of the total sample volume and incubated at room temperature for 0.5, 1, 5, 10, or 20 min. NPs were magnetically pelleted, the supernatant was removed, and NPs were resuspended in an enzymatic RNA extraction cocktail (*RNA*GEM, MicroGEM International, PCL, Charlottesville, VA) consisting of 88 μL of water, 10 μL of BLUE buffer, and 2 μL of *RNA*GEM enzyme solution prior to incubation for 5 min at 95 °C. Samples were also prepared with the RNeasy Mini Kit (Qiagen, Valencia, CA) according to the manufacturer's instructions. In-tube matrix effects were tested with clinical samples neat and diluted with fresh saliva to 1:1, 1:4, and 1:8. For comparison of eluates from the in-tube and on-disc methods, sample and elution volumes were decreased from 100 to 50 μL (44 μL of water, 5 μL of BLUE buffer, and 1 μL of *RNA*GEM enzyme solution); the NP input volume was adjusted to maintain a 20% concentration.

Device Design and Fabrication. Microdevice architecture was designed using AutoCAD software (Autodesk, Inc., Mill Valley, CA) and laser-ablated into thermoplastic substrates using a CO_2 laser (VLS 3.50, Universal Laser Systems, Scottsdale, AZ). The primary device consists of five poly(ethylene terephthalate) (PeT) layers (Film Source, Inc., Maryland Heights, MO). Capping layers 1 and 5 are composed of PeT, whereas primary fluidic layers 2 and 4 are composed of heat-sensitive adhesive (EL-7970-39, Adhesives Research, Inc., Glen Rock, PA)-coated PeT. Layer 3, composed of black PeT (bPeT) (Lumirror X30, Toray Industries, Inc., Chuo-ku, Tokyo, Japan), acts as an intervening layer between the two primary fluidic layers to permit laser valving.[19] Layers were aligned and heat-bonded using a laminator (UltraLam 250B, Akiles Products, Inc., Mira Loma, CA) according to the "print, cut, laminate" method, described elsewhere.[20] The poly(methyl methacrylate) (PMMA) accessory layer (1.5 mm thickness, McMaster Carr, Elmurst, IL) was affixed to layer 1 by a pressure-sensitive adhesive (PSA) transfer tape (MSX-7388, 3M, Saint Paul, MN), capped with PeT, and used to increase the chamber depth and fluid capacity.[18] Fluidic channels connecting microdevice chambers had a depth of approximately 100 μm and approximate widths between 400 and 500 μm.

Spin System Construction and Operation. Valve opening,[21] channel closures,[19] rotationally driving flow, and magnetic mixing[18] were enabled by in-house mechatronic systems regulated by 8-core microcontrollers (Propeller P8X32A-M44; Propeller, Inc., Rockland, CA) and custom programs written in *Spin*, Propeller's coding language, run from a laptop computer. On-disc heating was facilitated by a clamped, dual-Peltier system.

Power, Time, and Z-Height Adjustable Laser (PrTZAL) System. Laser valving events and rotationally driven flow were accomplished with the PrTZAL system, described elsewhere.[19] Active valving via a 638 nm laser diode occurred when the disc was stationary and situated under the laser at the corresponding radial distance from the center of rotation (r), measured in mm. To open the valves, the laser was positioned 15 mm above the disc, and irradiation occurred at 500 mW for 500 ms.[19] Channels were occluded by situating the disc 27 mm

https://doi.org/10.1021/acs.analchem.1c05215
Anal. Chem. 2022, 94, 3287−3295

below the laser and with a power output of 700 mW for 2500 ms. A DC brushless motor was used to drive device rotation, enabling fluidic control.

Dynamic Solid-Phase Extraction (dSPE) Platform. The dSPE platform[18] was used to impart external magnetic control of the paramagnetic affinity-capture hydrogel NPs for efficient mixing with both the SARS-CoV-2 samples and the enzymatic extraction reagents. The platform houses a PMMA disc (diameter = 150 mm, thickness = 1.50 mm) placed 7.50 mm above the sample disc platform and featuring two Neodymium magnets to generate the bRMF[18] that facilitates back-and-forth NP sweeping within a chamber with reversal of rotational direction.

On-Disc Enrichment and Enzymatic Extraction Protocol. Liquid sample (50 μL), enzymatic extraction cocktail (50 μL), and NPs (10 μL) were introduced to corresponding chambers via pipette loading. After actuation of valve 1, disc rotation drove the fluid from the sample input chamber to the central magnetic manipulation chamber (1500 g, 30 s). Here, SARS-CoV-2 virions were adsorbed to NPs during bRMF application for a total of 300 s, switching direction every 20 s. NPs were centrifugally pelleted (2000 g, 60 s) before valve 2 (r = 45.4 mm) was opened and supernatant was pumped (1500 g, 30 s) into the waste chamber. The channel upstream of the waste chamber was laser-sealed to prevent further fluid flow. Valve 3 was then opened to permit the lysis cocktail to flow (1500 g, 30 s) into the magnetic manipulation chamber for another mixing step. The central chamber was then heated to 95 °C for 1 min prior to NP pelleting (2000 g, 60 s). Sample elution to the viral RNA elution chamber occurred after the opening of valve 4 and disc rotation (1500 g, 30 s). The RNA eluate was then retrieved by pipette after puncturing the capping layer PeT.

Performance and Analysis of Dye Visualization Studies. Blue and yellow aqueous dye solutions were used to visually represent the sample and extraction cocktail, respectively. Device images were captured using an Epson Perfection V100 Photo desktop scanner (Seiko Epson Corporation, Suwa, Nagano Prefecture, Japan). Raw images were converted to HSB stacks using the Fiji ImageJ freeware and analyzed using the "crop-and-go" technique.[22] Briefly, the hue of a rectangular region of interest (ROI) within each chamber (n = 6) and parallel measurements were compared to control dye solutions of known constituency on-disc. Control solutions were comprised of serially diluted blue dye in yellow dye from 10% to 0% (each n = 3).

Real-Time Polymerase Chain Reaction. Detection of SARS-CoV-2 was accomplished using the Centers for Disease Control and Prevention (CDC) assay.[23] Per manufacturer's instructions, each 20 μL reaction was composed of 5 μL of TaqPath 1-Step RT-qPCR Master Mix, CG (Thermo Fisher Scientific, Waltham, MA), 1.5 μL of SARS-CoV-2 (2019-nCoV) CDC RUO N1 primer-probe mix (Integrated DNA Technologies, Coralville, IA), 8.5 μL of PCR-grade water (Molecular Biologicals International, Inc.), and 5 μL of eluate. For positive controls, the 2019-nCoV_N_ Positive Control plasmid (100 000 copies/μL, Integrated DNA Technologies) was diluted to 1000 copies/μL in PCR-grade water (Molecular Biologicals International, Inc.). All samples were run in triplicate on a QuantStudio 5 Real-Time PCR System with detection in the FAM channel (Thermo Fisher Scientific). Thermal conditions included reverse transcription (50 °C, 900 s), denaturation (95 °C, 180 s), 40 cycles of denaturation (95 °C, 3 s), and annealing (60 °C, 30 s), with a final hold step at 25 °C. The 60 °C annealing temperature was determined optimal over the manufacturer's recommended temperature of 55 °C previously.[13] Amplification was considered successful if the signal amplitude crossed the instrument-defined threshold, providing a C_t value, before the 40 cycle cutoff.

RESULTS AND DISCUSSION

The development of a μCD for virion enrichment and enzymatic RNA extraction from SARS-CoV-2 samples is described. Here, sample preparation required in-tube chemistry optimization to maximize the enrichment efficacy, assessed through a comparison with a commercial method. Furthermore, the effects of different sample matrices on preparation were evaluated. Successful μCD integration necessitated precise fluidic control to permit implementation of discrete unit operations. To demonstrate analytical performance, C_t values obtained via real-time RT-PCR amplification of extracted viral RNA were compared; because C_t values are indicative of relative starting concentrations, optimal conditions for sample preparation would produce more rapid amplification (i.e., lower C_t values). We show that virions can be effectively enriched from multiple matrices and lysed to release amplification-ready viral RNA by our method.

Sample Preparation Method for Viral Enrichment and Enzymatic Nucleic Acid Extraction. The sample preparation workflow (Figure 1) was optimized from a previously described protocol[13] to limit manual intervention, decrease total analysis time, and limit the risk for analyst exposure to pathogens. Magnetically actuated NPs were used for virion capture and isolation from clinical matrices.[24] Lysis of the viral envelope and liberation of RNA was accomplished with *RNA*GEM chemistry.[15] This single-step, enzyme-based extraction method does not require time- and labor-intensive column-purification and circumvents centrifugation by leveraging temperature control. Optimal release of nucleic acids is achieved at a temperature of 75 °C,[15] with termination of the reaction at 95 °C to diminish activity and prevent detection inhibition downstream.[25] The process time can be reduced by

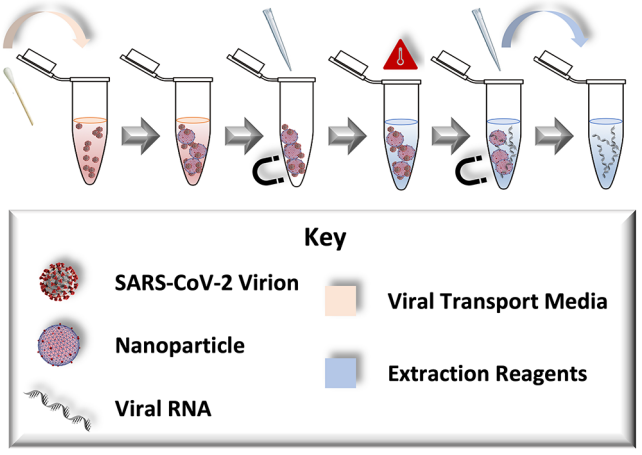

Figure 1. In-tube proposed sample preparation workflow. Enrichment from the sample leverages affinity NPs for virion adsorption. Following magnetic actuation and removal of the supernatant, RNA extraction is achieved in a PCR compatible buffer. The reaction mixture is heated to 95 °C before a second magnetic step and the pipette removal of the viral RNA eluate.

https://doi.org/10.1021/acs.analchem.1c05215
Anal. Chem. 2022, 94, 3287−3295

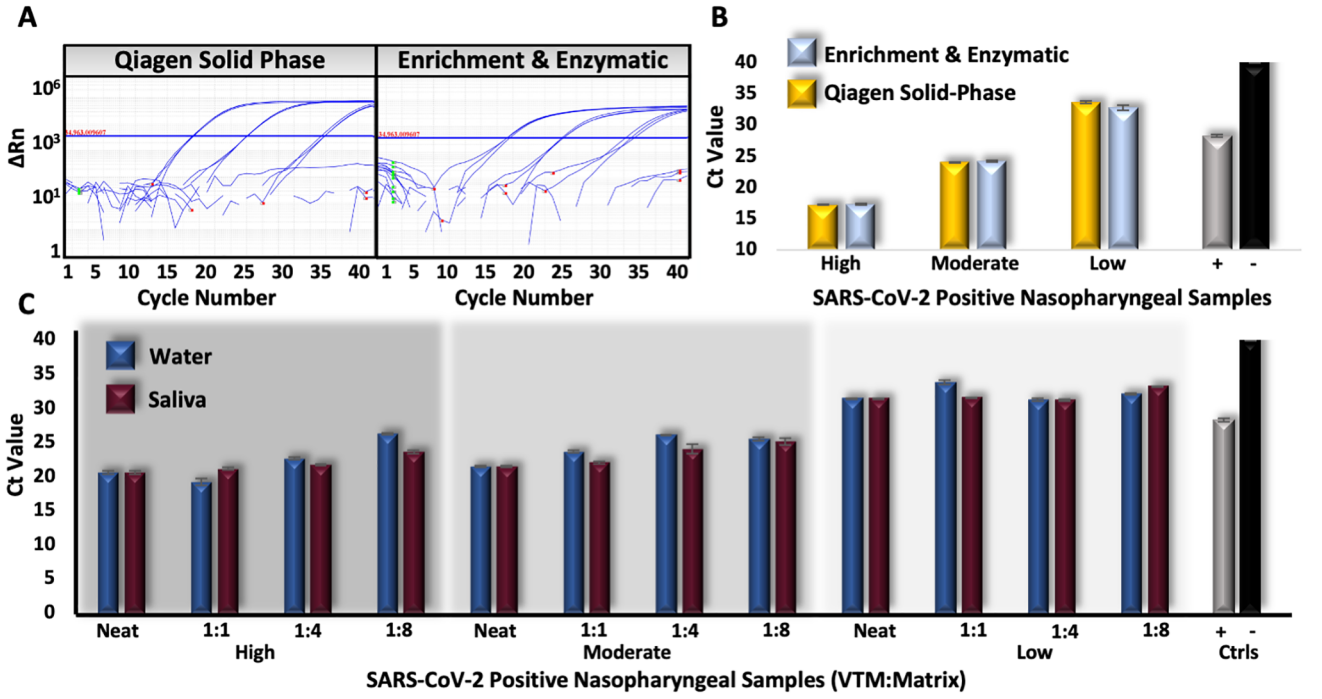

Figure 2. In-tube enrichment and enzymatic extraction optimization. (A, B) Clinical samples were extracted by the solid-phase or proposed method in-tube. No statistical differences were observed between C_t values resulting from amplification of eluates produced by either method. (C) Clinical samples were prepared neat and serially diluted in water (blue) and saliva (burgundy) in parallel. Resultant C_t values demonstrate average differences below two C_t units.

controlling the rate of heating and was decreased here to ∼5 min. Amplification of the target RNA after NP enrichment and enzymatic sample preparation was successful, indicating these processes could be coupled.

For virion enrichment, parameters including NP input volume and incubation time were optimized with consideration given to resultant C_t values, reagent conservation, and total analysis time. First, parallel aliquots from three positive clinical samples at high, moderate, and low concentrations were analyzed with NP percentages between 5 and 50%. Optimal NP input volume was determined to be 20% of the total sample volume, as 5% and 10% enrichment parameters were found to produce higher relative C_t values, indicating lower postextraction RNA concentrations, whereas input volumes higher than 20% did not exhibit appreciably different C_t values across sample concentrations (Figure S1 in the Supporting Information). This NP concentration was used to determine the optimal NP incubation time from 30 s to 20 min using clinical samples with variable relative titers. The ideal incubation time was determined to be 5 min, with all others producing either significantly higher or comparable C_t values; for instance, low-concentration samples incubated for 10 and 20 min show the same mean C_t units (Figure S2). Enrichment conditions both in-tube and with the μCD were dictated by these results.

To compare enriched *RNA*GEM eluates with a commercial technique, samples were prepared in-tube using the proposed method and a Qiagen solid-phase method for RNA extraction. RNA isolated from samples with relatively low, moderate, and high viral titers using both methods in parallel was amplified (Figure 2A), and resultant C_t values were compared (Figure 2B). A two-way analysis of variance (ANOVA) with replication indicates the null hypothesis (equivalence of means) could not be rejected ($\alpha = 0.05$, p-value = 0.116); stated another way, the C_t values produced by amplification of RNA prepared using both methods were statistically similar at each viral titer. That is, after preparation by a column-based, labor-intensive approach and the simplified method described, eluates produce the same amplification results.

To demonstrate applicability of this method to various types of clinical samples, we evaluated whether the presence of a biological matrix, namely, saliva, affected sample preparation. Using our in-tube method, we tested parallel aliquots from clinical samples, neat and diluted in either water or saliva, at various titers (Figure 2C). We hypothesized that because NP enrichment permits matrix removal prior to RNA extraction, any adverse effects of the matrix on downstream amplification, and ultimately detection sensitivity, would be mitigated. Although resultant C_t values appeared comparable at each dilution factor, separate two-way ANOVA tests for high-, moderate-, and low-concentration samples demonstrated statistical differences in C_t values across matrices ($\alpha = 0.05$, p-values = 0.007, 1.061×10^{-5}, and 0.017, respectively). However, mean differences between C_t values from each donor sample diverge by less than 2 units (1.150−1.854). Furthermore, differences between C_t values across sample concentrations, matrices, and dilutions appear to be stochastic, with no clear trend suggesting one matrix as preferable over the other. Moreover, results indicate no appreciable difference between detection results from samples diluted in either water or saliva matrices.

Adaptation to the Rotational Microdevice. The μCD was designed with a view toward increased throughput and includes six identical domains for parallel, multiplexed sample preparation (Figure 3A,B). Within a single domain, NP enrichment and enzymatic lysis occur in the centrally located

https://doi.org/10.1021/acs.analchem.1c05215
Anal. Chem. 2022, 94, 3287−3295

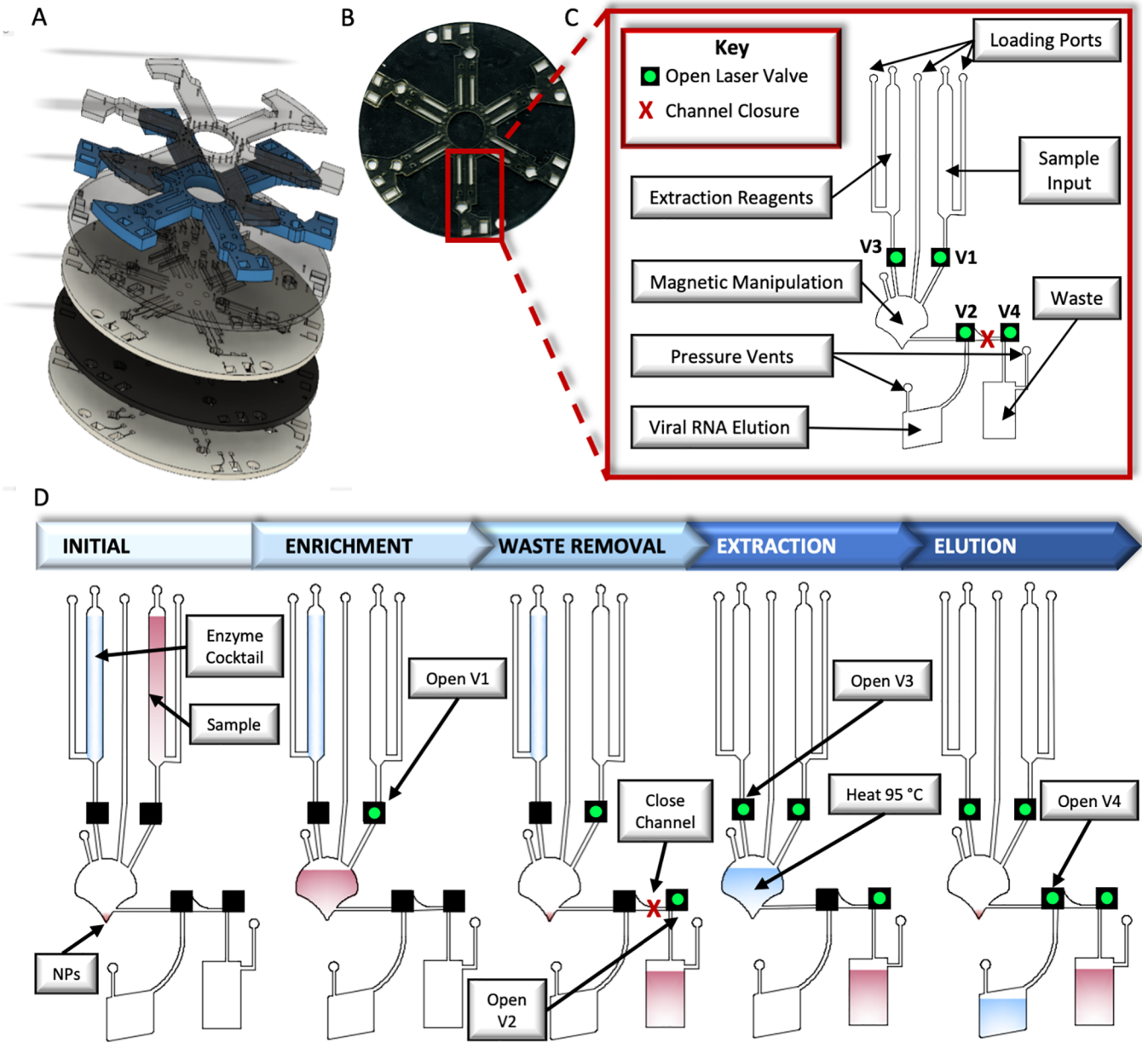

Figure 3. Sample preparation μCD architecture. (A) Exploded depiction of the 5-layer polymeric disc and capping layer to enable increased chamber volumes, affixed to the disc by PSA and capped with PeT. (B, C) Top view of μCD and one labeled domain depicting sample chambers, fluidic channels, pressure vents, laser valves, and reagent loading ports. (D) Sequential unit operations performed using the μCD, including reagent and sample loading, enrichment, waste removal, extraction, and viral RNA elution.

magnetic manipulation chamber. This "concave-shaped"[18] chamber features a distal vertex, designed to retain magnetic NPs during supernatant removal and, ultimately, RNA elution. The liquid sample, suspended NPs, and the enzymatic extraction cocktail were loaded into the sample input, magnetic manipulation, and extraction reagents chambers, respectively (Figure 3D). Comprehensive virion capture during NP enrichment of the sample was facilitated through bRMF-induced back-and-forth NP "sweeping" (Figure 3D).

The sample/NP mixture was subjected to the bRMF for 5 min, the same interval determined to provide enrichment in-tube (Figure S2). NPs, now with adsorbed virions, were centrifugally pelleted into the chamber vertex to maximize retention for supernatant removal to the waste chamber (Figure 3D). NPs were resuspended via introduction of the enzymatic lysis cocktail to the magnetic manipulation chamber. Lysis of adsorbed virions was enhanced via the bRMF to increase turbulence and promote more frequent interactions between trapped virions and lysis enzymes than possible under purely diffusive conditions (Figure 3D). Assay adaptation to the microscale allowed for shortened incubation times relative to in-tube methods due, in part, to increased surface area to volume ratios.[26] This advantage was essential for our assay because high-temperature incubations greater than 3 min were not optimal for our thermally bonded polymeric devices. Thus, the optimized in-tube protocol using a 5 min lysis incubation could not be directly translated to the μCD assay. However, a reduced lysis dwell time of only 1 min showed successful in-

https://doi.org/10.1021/acs.analchem.1c05215
Anal. Chem. 2022, 94, 3287−3295

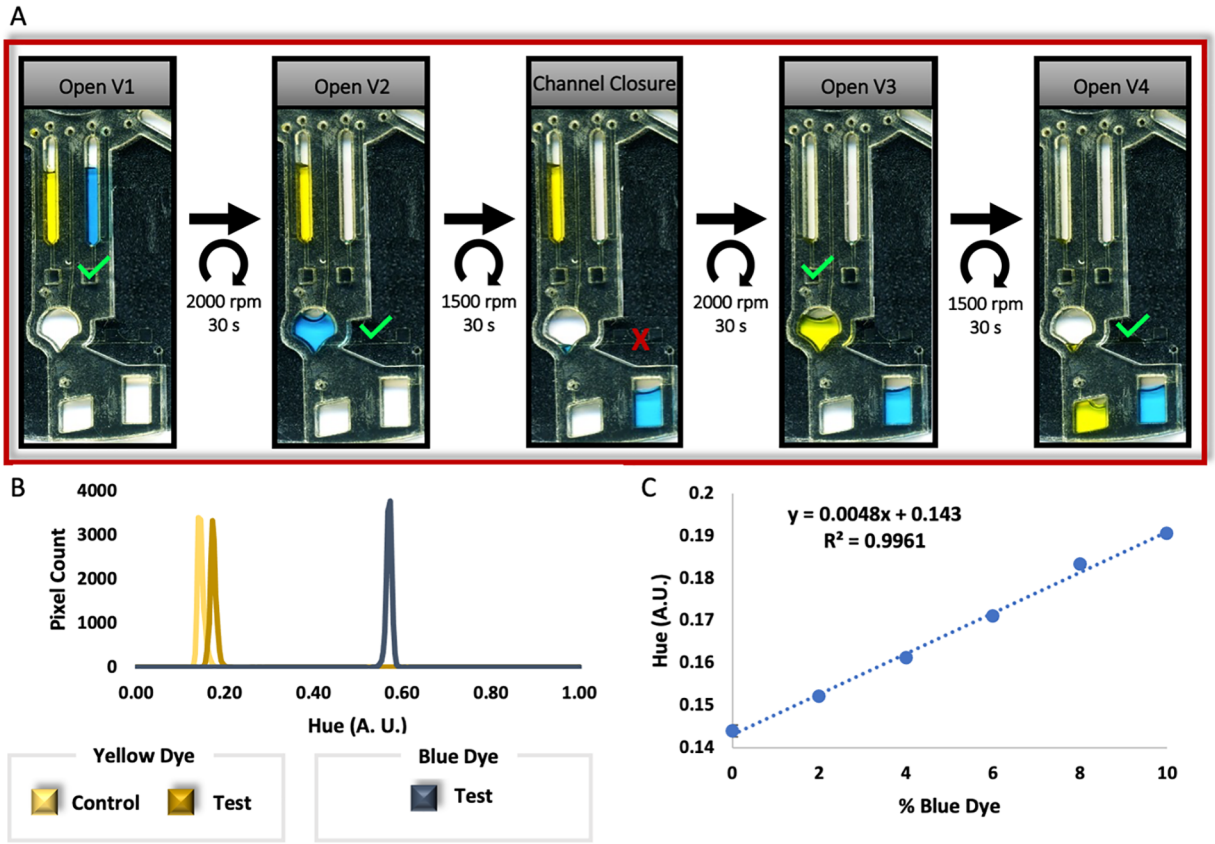

Figure 4. Sample preparation μCD dye study. (A) One representative μCD domain depicting the progress of a dye study (n = 6). Aqueous blue and yellow dye solutions represent the sample and extraction cocktail, respectively. (B) Line graph depicting the hue of both dyes following the μCD protocol, compared to control dye solutions. The increased hue measured from the yellow dye after the assay represents the carryover of the blue dye (sample matrix) into the final eluate (yellow fraction). (C) Calibration curve of the hue against the percentage of blue dye mixed with yellow solution used to calculate the magnitude of sample carryover into the final eluate observed during the μCD assay.

tube RNA isolation from clinical samples. A 2-way ANOVA comparing C_t values indicated RNA yields were statistically similar after 5- and 1-min incubations across all sample concentrations (α = 0.05, p-value = 0.2968) (Figure S3). Thus, all μCD lysis reactions had a duration of only 1 min. Finally, NPs were centrifugally pelleted, and the eluate was rotationally driven into the viral RNA elution chamber, from which it could be collected and amplified with no further purification required (Figure 3D).

***μ*CD Fluidic Control and Assessment of Eluate Purity.** The reliability of μCD method was dependent on reproducible performance of the sequential unit operations in the requisite order. Furthermore, the carryover of the matrix into the RNA eluate confers detrimental effects on the performance of downstream real-time RT-PCR.[27] To evaluate the μCD architecture and determine whether this type of inhibition is likely to occur in our system, dye studies were completed to colorimetrically characterize the matrix presence in the on-disc eluate (Figure 4A,B). Here, aqueous blue and yellow dye solutions were used to represent the sample and extraction cocktail, respectively. The dyes were moved throughout each domain according to the assay workflow, with all valve openings and channel closures reproducibly operating as expected (Figure 4B). Quantification of matrix prevalence in the eluate was enabled by collecting empirical measurements of the hue, the circular variable that represents a color within the visible portion of the electromagnetic spectrum.[22] The hue of the yellow dye in the eluate chamber after the completion of the assay workflow (0.175 ± 0.003) was statistically significantly higher than that of pure yellow dye (0.147 ± 0.004), according to an unpaired t test for means (α = 0.05, two-tailed p-value <0.0001). This upward shift in hue was attributed to contamination with the blue dye (hue = 0.571 ± 0.002), which reflects the carryover of the matrix into the viral RNA eluate (Figure 4C). Mixing between fractions was not unexpected; the magnetic manipulation chamber geometry was designed to retain NPs in the vertex extending radially outward below the elution channel for maximized RNA recovery, as discussed above.[18] Simultaneous capture of fluid in this vertex, and ultimately carryover into the eluate, was unavoidable. To characterize the extent of matrix carryover, hue measurements taken from the μCD eluate fraction were compared to dye mixtures of known composition. Specifically, colorimetric analysis of serially diluted dye standards (blue in yellow) demonstrated a strong linear correlation between increases in the hue and in the prevalence of the blue dye (R^2 = 0.996) (Figure 4D). This relationship was used to calculate that the final eluate is comprised of 6.58 ± 0.72% blue dye, or crude sample matrix. However, NPs were not included in this dye study; we anticipate that the prevalence of sample matrix in viral RNA eluates would be much lower. During preparation of real samples, NPs would occupy the chamber vertex during supernatant flow to waste, sterically excluding fluid. Therefore,

https://doi.org/10.1021/acs.analchem.1c05215
Anal. Chem. 2022, 94, 3287−3295

we concluded that on-disc viral RNA eluates would contain only minimal matrix, which would likely not inhibit PCR.

SARS-CoV-2 Full-Process Controls and Clinical Samples. Experimental results from replicate dye studies indicated effectual architectural features and reliable fluidic control. Furthermore, in-tube studies indicated that our RNA preparation workflow produced comparable results to a gold-standard method. To demonstrate successful μCD adaptation, SARS-CoV-2 reference material was serially diluted and prepared in parallel using the proposed method in-tube and with the μCD. Briefly, this reference material was selected because it features an extractable viral protein coat encapsulating the RNA, and thus may serve as a full-process control. C_t values obtained from in-tube and μCD extractions were compared to those from the 2019-nCoV Positive Control plasmid, diluted to equivalent concentrations (Figure 5A). We hypothesized that samples prepared by both methods would produce equivalent C_t values and likewise be similar to cDNA plasmid positive controls, indicating successful automation with the μCD and good extraction efficiency, respectively. According to one-way ANOVA tests to analyze the equivalence of means, for samples prepared at 50 and 25 copies/μL, the null hypothesis could not be rejected (α = 0.05, p-values = 0.3306 and 0.5281, respectively), suggesting C_t values were statistically similar. Thus, at these concentrations, RNA isolation performs comparably in-tube and in the μCD, producing similar RNA yields. Furthermore, statistical similarity between extracted RNA C_t values with that of the plasmid positive control, which does not require enrichment or extraction, suggests highly efficient *RNA*GEM extraction both in-tube and on-disc. Conversely, analysis of 100 copies/μL samples indicated a statistically significant difference between the three conditions (α = 0.05, p-value <0.0001). Upon closer examination using a Tukey's test, more variation exists between the prepared samples and the plasmid positive control than between the two preparation methods. The mean C_t values between the in-tube and on-disc methods were 3.711 and 3.134 units different from that of the plasmid positive control, respectively. For contrast, a comparison of the C_t values obtained from in-tube and μCD preparation reveals a mean difference of only 0.577 units, indicating adaptation to the μCD was not detrimental to the sample preparation chemistry. Here, we have demonstrated that, with full-process controls, sample preparation by the μCD produces amplification-ready RNA comparable to that by the in-tube method.

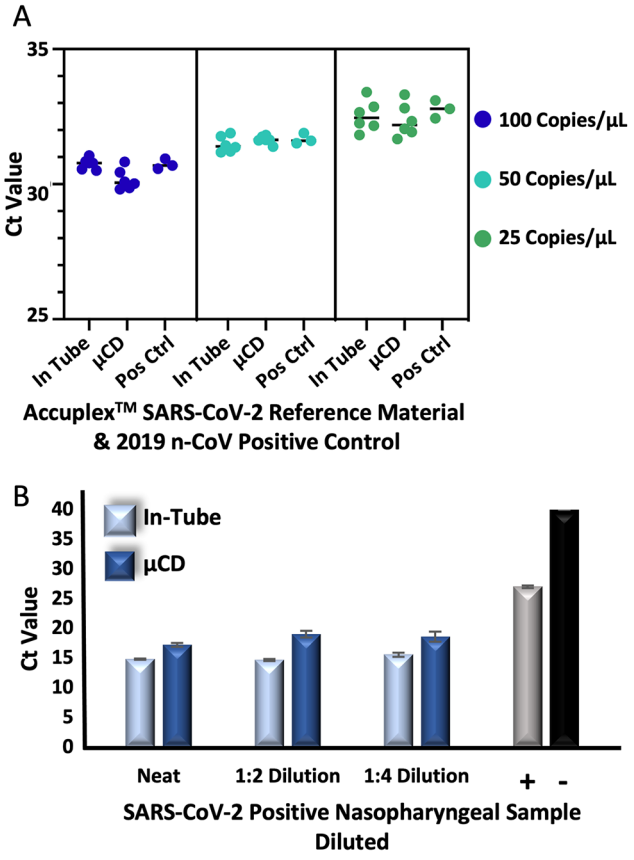

Figure 5. Testing of the μCD method. (A) Full-process SARS-CoV-2 control was extracted in duplicate neat and diluted in water with the in-tube and μCD methods. Resultant C_t value comparisons suggest statistically significant differences at 100 copies/μL, but not at 50 and 25 copies/μL. (B) A clinical sample was extracted neat and diluted in water using both methods. Resultant eluates produced higher C_t values with the μCD method.

Next, to evaluate the method's capacity for the preparation of clinical samples, positive samples were prepared via the μCD workflow. Real-time RT-PCR amplification of RNA isolated from VTM samples neat and diluted (1:2, 1:4) was successful for all samples prepared using both the in-tube and μCD methods. Notably, eluates with different dilution factors exhibit similar C_t values between methods, a phenomenon observed previously by our group that has been attributed to the viral saturation of NPs at high viral titers and that does not prevent SARS-CoV-2 identification.[13] Still, resultant C_t values indicated larger differences between the eluates generated across methods using real clinical samples compared to those observed from reference material and positive controls (Figure 5B). On average, C_t values resulting from amplification of μCD isolates were 3.266 units higher than those prepared in-tube. We suspect these results diverge from those generated when comparing the full-process control as a direct result of the presence of a residual matrix. Recall that, with the μCD method, the carryover of some matrix is expected.

Performance with Multiple Sample Matrices. To this point, dilutions of full-process controls and VTM from nasopharyngeal swabs were prepared in water. We considered whether this may have contributed to the higher C_t values and sought to investigate this further by instead diluting the samples in matrices negative for SARS-CoV-2. This way, the matrix would ostensibly remain consistent, while the input concentration changed. To control for the concentration, undiluted full-process SeraCare controls (100 copies/μL) were again processed in-tube and with the μCD (Figure 6). In parallel, samples were diluted in the nasopharyngeal VTM matrix, prepared by both methods, and amplified via real-time RT-PCR (Figure 6). Unpaired t tests indicate a statistical difference between replicate C_t values at concentrations of 100, 50, and 25 copies/μL (α = 0.05, p-values = 0.0086, 0.0158, and 0.0026, respectively). Interestingly, the average C_t value difference between conditions at all concentrations was less than 1 unit (~0.9122), which is much less variable than those of samples diluted in water (Figure 5A). We hypothesize the increased success with samples diluted in VTM can be attributed to the stabilizing properties of the medium;[28] furthermore, studies have demonstrated diminished stability for other coronavirus strains suspended in water.[29]

https://doi.org/10.1021/acs.analchem.1c05215
Anal. Chem. 2022, 94, 3287−3295

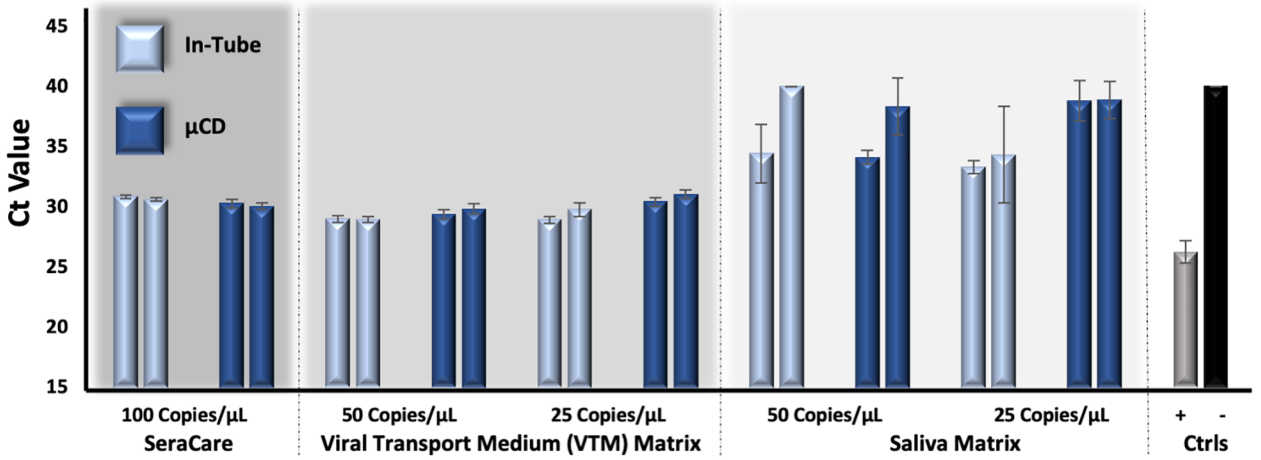

Figure 6. Method performance with multiple sample matrices. Full-process SARS-CoV-2 control was extracted in duplicate by the in-tube and μCD methods neat and diluted in two different matrices: (1) a negative clinical nasopharyngeal sample suspended in VTM and (2) fresh saliva. Statistical differences were observed between resultant C_t values across all concentrations and conditions analyzed; notably, average C_t value differences were less than 1 unit with VTM samples prepared by either method.

We next evaluated the capacity for the μCD to process saliva, which has recently garnered much attention as an alternative sampling type for SARS-CoV-2 detection, given its noninvasive collection.[30] We hypothesized the increased viscosity and complexity of saliva may pose analytical challenges. This was observed when samples prepared in saliva demonstrated higher C_t values, and thus diminished amplification sensitivity, compared to the VTM-diluted samples (Figure 6). For example, at 25 copies/μL, average C_t values for samples prepared in VTM were ~30.05, while those prepared in saliva were ~36.35. Additionally, the disparity in performance between in-tube and μCD preparation was more pronounced in the analysis of saliva compared to that of VTM (Figure 6). Considering the 25 copies/μL samples, amplification of μCD extracts from VTM exhibited diminished sensitivity of only ~1.38 C_t units relative to RNA prepared in-tube; analogous samples diluted in saliva showed a larger difference.

CONCLUSIONS

We report a rotationally driven microfluidic method for the enrichment and enzymatic RNA extraction of SARS-COV-2 clinical samples in under 15 min. The μCD is capable of processing up to six samples in parallel. Each domain can accommodate as much as 50 μL of input, which serves to ease the difficulty in bridging the macro- to microinterface, a persistent obstacle encountered in the development of microfluidic diagnostics.[31] Beyond the manual addition of clinical sample and reagents, all fluidic steps were automated to minimize user intervention, ease assay automation, and limit analyst exposure to viral pathogens. Integration of this method was facilitated by both the durability of the affinity-bait NPs and the versatility of the lysis chemistry.[8,13] Incorporation of enrichment enabled the removal of the virion from a matrix, likely to contain sample constituents that would negatively impact detection. The automation of this process on the μCD necessitated the design of an infrastructure capable of removing residual supernatant matrix without the use of an internal filter to sequester virion-containing NPs. To permit this, we used rotational force to our advantage, driving NPs to the vertex[18] of the requisite chamber for retention during supernatant flow to waste. We used dye studies to confirm that only a small amount of residual matrix remains in the final RNA eluate.

Experimentally optimized enrichment parameters were paired with a one-step enzymatic extraction method to permit rapid provision of PCR-ready RNA. In-tube, the workflow demonstrated comparable performance to a gold-standard analytical technique, producing statistically similar C_t values with clinical samples at various concentrations diluted in both water and saliva. Thus, our approach exhibits applicability to clinically relevant matrices. Using the μCD method for preparation, we reliably detected SARS-CoV-2 downstream with full-process controls and positive nasopharyngeal swabs suspended in VTM; in some cases, a comparison of C_t values indicated no statistical difference between eluates produced by the in-tube and μCD methods. Viral RNA was also successfully detected from saliva samples prepared by the μCD method, emphasizing the method's ability to handle sample matrices commonly encountered in clinical diagnostics.

ASSOCIATED CONTENT

Supporting Information

The Supporting Information is available free of charge at https://pubs.acs.org/doi/10.1021/acs.analchem.1c05215.

Bar graph depicting optimization of nanoparticle percentage; bar graph depicting optimization of nanoparticle incubation time; bar graph showing the effect of shortening heated extraction times (PDF)

AUTHOR INFORMATION

Corresponding Author

Rachelle Turiello − *Department of Chemistry, University of Virginia, Charlottesville, Virginia 22904, United States;* orcid.org/0000-0001-5110-2304; Email: rat3a@virginia.edu, rachelleturiello@gmail.com

Authors

Leah M. Dignan − *Department of Chemistry, University of Virginia, Charlottesville, Virginia 22904, United States;* orcid.org/0000-0002-4109-4205

https://doi.org/10.1021/acs.analchem.1c05215
Anal. Chem. 2022, 94, 3287−3295

Brayton Thompson − *Department of Chemistry, University of Virginia, Charlottesville, Virginia 22904, United States*
Melinda Poulter − *Clinical Microbiology, University of Virginia, Charlottesville, Virginia 22904, United States*
Jeff Hickey − *MicroGEM International, PLC, Charlottesville, Virginia 22903, United States*
Jeff Chapman − *MicroGEM International, PLC, Charlottesville, Virginia 22903, United States*
James P. Landers − *Department of Chemistry, Mechanical and Aerospace Engineering, and Pathology, University of Virginia, Charlottesville, Virginia 22904, United States; MicroGEM International, PLC, Charlottesville, Virginia 22903, United States*

Complete contact information is available at: https://pubs.acs.org/10.1021/acs.analchem.1c05215

Notes

The authors declare the following competing financial interest(s): Many of the authors listed here are stakeholders in MicroGEM International, PLC. Further, this work was performed as part of a collaboration with MicroGEM, who was awarded the NIH RADx contract. While the work here is not currently a planned commercialization product for MicroGEM, it was carried out at the University of Virginia (UVA) and the UVA Licensing and Ventures Group (LVG) offers technology originating from Landers Laboratory to MicroGEM for potential licensing.

■ ACKNOWLEDGMENTS

The authors acknowledge MicroGEM International, PLC, for their guidance and support of this project. In addition, we thank 3M for their contribution of polymeric materials. Finally, we thank the University of Virginia Licensing and Ventures Group for their engagement with the technology and protection of the associated intellectual property.

■ REFERENCES

(1) Guan, W.; Ni, Z.; Hu, Y.; Liang, W.; Ou, C.; He, J.; Liu, L.; Shan, H.; Lei, C.; Hui, D. S. C.; Du, B.; Li, L.; Zeng, G.; Yuen, K.-Y.; Chen, R.; Tang, C.; Wang, T.; Chen, P.; Xiang, J.; Li, S.; Wang, J.; Liang, Z.; Peng, Y.; Wei, L.; Liu, Y.; Hu, Y.; Peng, P.; Wang, J.; Liu, J.; Chen, Z.; Li, G.; Zheng, Z.; Qiu, S.; Luo, J.; Ye, C.; Zhu, S.; Zhong, N. *N Engl J. Med.* **2020**, *382*, 1708−1720.
(2) Uhteg, K.; Jarrett, J.; Richards, M.; Howard, C.; Morehead, E.; Geahr, M.; Gluck, L.; Hanlon, A.; Ellis, B.; Kaur, H.; Simner, P.; Carroll, K. C.; Mostafa, H. H. *Journal of Clinical Virology* **2020**, *127*, 104384.
(3) Ali, N.; Rampazzo, R. de C. P.; Costa, A. D. T.; Krieger, M. A. *BioMed. Research International* **2017**, *2017*, 1−13.
(4) Esbin, M. N.; Whitney, O. N.; Chong, S.; Maurer, A.; Darzacq, X.; Tjian, R. *RNA* **2020**, *26*, 771−783.
(5) Katevatis, C.; Fan, A.; Klapperich, C. M. *PloS ONE* **2017**, *12*, e0176848.
(6) Mina, M. J.; Parker, R.; Larremore, D. B. *N Engl J. Med.* **2020**, *383*, e120.
(7) Hall, R. J.; Wang, J.; Todd, A. K.; Bissielo, A. B.; Yen, S.; Strydom, H.; Moore, N. E.; Ren, X.; Huang, Q. S.; Carter, P. E.; Peacey, M. *Journal of Virological Methods* **2014**, *195*, 194−204.
(8) Shafagati, N.; Narayanan, A.; Baer, A.; Fite, K.; Pinkham, C.; Bailey, C.; Kashanchi, F.; Lepene, B.; Kehn-Hall, K. *PloS Negl Trop Dis* **2013**, *7*, No. e2296.
(9) Barclay, R.; Akhrymuk, I.; Patnaik, A.; Callahan, V.; Lehman, C.; Andersen, P.; Barbero, R.; Barksdale, S.; Dunlap, R.; Goldfarb, D.; Jones-Roe, T.; Kelly, R.; Kim, B.; Miao, S.; Munns, A.; Munns, D.; Patel, S.; Porter, E.; Ramsey, R.; Sahoo, S.; Swahn, O.; Warsh, J.; Kehn-Hall, K.; Lepene, B. Nanotrap® Particles Improve Detection of SARS-CoV-2 for Pooled Sample Methods, Extraction-Free Saliva Methods, and Extraction-Free Transport Medium Methods. *bioRxiv (Microbiology)*, December 30, 2020 (accessed January 2021), DOI: 10.1101/2020.06.25.1725.10.
(10) Maddu, N. Functions of Saliva. In *Saliva and Salivary Diagnostics*; Gokul, S., Ed.; IntechOpen: 2019.
(11) Schrader, C.; Schielke, A.; Ellerbroek, L.; Johne, R. *J. Appl. Microbiol.* **2012**, *113* (5), 1014−1026.
(12) Luchini, A.; Geho, D. H.; Bishop, B.; Tran, D.; Xia, C.; Dufour, R. L.; Jones, C. D.; Espina, V.; Patanarut, A.; Zhou, W.; Ross, M. M.; Tessitore, A.; Petricoin, E. F.; Liotta, L. A. *Nano Lett.* **2008**, *8* (1), 350−361.
(13) Dignan, L. M.; Turiello, R.; Layne, T. R.; O'Connell, K. C.; Hickey, J.; Chapman, J.; Poulter, M. D.; Landers, J. P. *Anal. Chim. Acta* **2021**, *1180*, 338846.
(14) Coolbear, T.; Eames, C. W.; Casey, Y.; Daniel, R. M.; Morgan, H. W. *Journal of Applied Bacteriology* **1991**, *71* (3), 252−264.
(15) Moss, D.; Harbison, S.-A.; Saul, D. J. *Int. J. Legal Med.* **2003**, *117* (6), 340−349.
(16) Strohmeier, O.; Keller, M.; Schwemmer, F.; Zehnle, S.; Mark, D.; von Stetten, F.; Zengerle, R.; Paust, N. *Chem. Soc. Rev.* **2015**, *44* (17), 6187−6229.
(17) Tian, F.; Liu, C.; Deng, J.; Han, Z.; Zhang, L.; Chen, Q.; Sun, J. *Sci. China Chem.* **2020**, *63* (10), 1498−1506.
(18) Dignan, L. M.; Woolf, M. S.; Tomley, C. J.; Nauman, A. Q.; Landers, J. P. *Anal. Chem.* **2021**, *93*, 7300.
(19) Woolf, M. S.; Dignan, L. M.; Lewis, H. M.; Tomley, C. J.; Nauman, A. Q.; Landers, J. P. *Lab Chip* **2020**, *20* (8), 1426−1440.
(20) Thompson, B. L.; Ouyang, Y.; Duarte, G. R. M.; Carrilho, E.; Krauss, S. T.; Landers, J. P. *Nat. Protoc* **2015**, *10* (6), 875−886.
(21) Garcia-Cordero, J. L.; Kurzbuch, D.; Benito-Lopez, F.; Diamond, D.; Lee, L. P.; Ricco, A. J. *Lab Chip* **2010**, *10* (20), 2680.
(22) Woolf, M. S.; Dignan, L. M.; Scott, A. T.; Landers, J. P. *Nat. Protoc* **2021**, *16* (1), 218−238.
(23) Freire-Paspuel, B.; Garcia-Bereguiain, M. *Int. J. Infect. Dis.* **2021**, *102*, 14−16.
(24) Xu, W.; Xu, N.; Zhang, M.; Wang, Y.; Ling, G.; Yuan, Y.; Zhang, P. *Acta Biomater.* **2022**, *138*, 57−72.
(25) Lounsbury, J. A.; Coult, N.; Miranian, D. C.; Cronk, S. M.; Haverstick, D. M.; Kinnon, P.; Saul, D. J.; Landers, J. P. *Forensic Sci. Int. Genet.* **2012**, *6* (5), 607−615.
(26) Zhang, Y.; Ozdemir, P. *Anal. Chim. Acta* **2009**, *638* (2), 115−125.
(27) Kirkland, P. D.; Frost, M. J. *Pathology* **2020**, *52* (7), 811−814.
(28) Perchetti, G. A.; Huang, M.-L.; Peddu, V.; Jerome, K. R.; Greninger, A. L. *J. Clin Microbiol* **2020**, *58*, 8.
(29) Carraturo, F.; Del Giudice, C.; Morelli, M.; Cerullo, V.; Libralato, G.; Galdiero, E.; Guida, M. *Environ. Pollut.* **2020**, *265*, 115010.
(30) Ceron, J.; Lamy, E.; Martinez-Subiela, S.; Lopez-Jornet, P.; Capela-Silva, F.; Eckersall, P.; Tvarijonaviciute, A. *JCM* **2020**, *9* (5), 1491.
(31) Fredrickson, C. K.; Fan, Z. H. *Lab Chip* **2004**, *4* (6), 526.